Available online at www.sciencedirect.com

ScienceDirect

IFAC PapersOnline CONFERENCE PAPER ARCHIVE

IFAC PapersOnLine 52-15 (2019) 253–258

Modeling of liquid sloshing with application in robotics and automation

Markus Schörgenhumer* Andreas Eitzlmayr**

**Linz Center of Mechatronics GmbH, Area Mechanics&Control, Linz, Austria (e-mail: markus.schoergenhumer@lcm.at)*

*** Linz Center of Mechatronics GmbH, Area Mechanics&Control, Linz, Austria (e-mail:andreas.eitzlmayr@lcm.at)*

Abstract: Liquid sloshing is a free surface flow phenomenon with particular impact in applications such as dynamics of vehicles, ships or aircrafts (e.g. sloshing in tanks), solutions for vibration damping (e.g. tuned liquid mass dampers), as well as in industrial automation and robotic systems (e.g. handling of liquid-filled vessels). Whether sloshing effects are utilized to reduce vibrations or, on the contrary, introduce disturbing forces to the system, the understanding of the liquid sloshing dynamics is crucial to obtain the respective desired system behavior. To this end, due to the complex dynamic effects, numerical methods are vital means for analysis and optimization. In the present work, we focus on the transport and handling of liquid-filled containers in the context of robotics and automation, analyzed using the method Smoothed Particle Hydrodynamics (SPH). The properties and potential of the chosen numerical approach are investigated and evaluated by examples from literature, and several extensions over conventional SPH implementations are proposed in order to enhance accuracy and robustness.

Keywords: liquid sloshing, tank sloshing, sloshing dynamics, smoothed particle hydrodynamics, density filtering, volume conservation

1. INTRODUCTION

The sloshing motion of fluids inside partially filled containers plays a crucial role in various fields of engineering and applications in today's automated industrial processes (cf., eg., Ibrahim et al. (2001)). Be it the sloshing of fuel in tanks of vehicles, air- or space crafts (see, e.g., Toumi et al. (2009)), the automated handling of liquid-filled vessels (Yano et al. (2001), Moriello et al. (2018)), or vibration dampers based on liquid masses (see, e.g., Gao et al. (1997)), in any case a complex free surface flow is coupled with a mechanical system. The forces due to the sloshing motion of the liquid may have a significant impact on the dynamics and control of vehicles or automated systems, can impair mechanical strength and fatigue, or may even be utilized in a beneficial manner. A detailed understanding of liquid sloshing and the dynamics of the coupled system is a prerequisite for a successful system design, with optimization objectives specific to the individual application. In the fields of automation and robotics, when moving liquid-filled vessels, the goal is typically to suppress sloshing effects as far as possible while meeting constraints on process timing, throughput, or system dynamics. The motivation of the present work lies in that context – the understanding, design, optimization and control of such systems supported by detailed offline- and efficient real-time models.

Whereas extensive theory and analytical findings exist on liquid sloshing dynamics (see, for instance, Ibrahim (2005)), approaches based on numerical modelling and simulation offer more detailed insights, particularly in case of complex system settings, trajectories of motion, or vessel geometries. A variety of numerical methods has been employed to simulate and study sloshing problems (see, e.g., Rebouillat and Liksonov (2010)), ranging from mesh-based methods such as the finite element method for two fluid phases using level-set techniques (Battaglia et al. (2018)), conventional finite volume approaches employing volume of fluid (VoF) techniques (Konopka et al. (2018)), hybrid grid-based methods (Chentanez and Müller (2011)), to meshless techniques such as the Smoothed Particle Hydrodynamics (SPH) (Shao et al. (2012), Green and Peiró (2018)) or the Moving Particle Semi-implicit Method (Fonfach (2016)). The main advantage of Lagrangian particle-based methods over mesh-based approaches is that free surface flows and sloshing effects – also in case of complex geometries or motion – can be captured naturally without the need of explicitly keeping track of the free surface (e.g., by level-set techniques, VoF approaches, two-phase modelling).

In the present work, we employ the particle method SPH which we have already successfully applied to various problems of fluid-structure interaction (FSI) by a coupling with flexible multibody systems (see, e.g., Schörgenhumer at al. (2013), Schörgenhumer and Humer (2018)) – and, in fact, liquid sloshing in applications of robotic and automation systems belongs to the class of FSI problems. Special focus lies on the modelling of the wall boundary conditions and techniques to enhance numerical stability and consistency.

The paper is organized as follows: In Section 2, the numerical method including the implemented extensions is described. In Section 3, it is applied to two test cases from literature in order to validate the approach, show its potential, and study

10.1016/j.ifacol.2019.11.683

its accuracy, robustness, as well as certain numerical effects. Section 4 summarizes the conclusions on the results and gives an outlook on current and future research activities.

2. METHODOLOGY

2.1 Smoothed Particle Hydrodynamics (SPH)

The main principle of the meshless method SPH is to discretize a continuum by a set of particles in an unstructured, but on average homogenously distributed way. To each particle, a certain mass and the field variables relevant to the respective problem are assigned, such as velocity, density, pressure, and temperature in case of thermo-fluid dynamics, or measures of strain and stress in solid mechanics. Any field variable $f(\boldsymbol{r})$ at a given point $\boldsymbol{r}$ in the problem domain is first approximated by a weighted interpolation of the integral form

$$f(\boldsymbol{r}) \approx \int_{|\boldsymbol{r}-\boldsymbol{r}'|\leq 2h} f(\boldsymbol{r}) W(|\boldsymbol{r}-\boldsymbol{r}'|, h) d^3\boldsymbol{r}', \tag{1}$$

on a spherical domain of radius $2h$ around the point $\boldsymbol{r}$ (i.e., the kernel support domain), with h denoting the so-called smoothing length and $W(|\boldsymbol{r}-\boldsymbol{r}'|, h)$ the kernel function. Among a variety of kernel functions with compact support, cf., e.g., Gomez-Gesteira (2010), the quintic polynomial Wendland kernel (Wendland (1995))

$$W(q,h) = \frac{21}{256\pi h^3}\begin{cases}(2-q)^4(1+2q) & \text{for } q \in [0,2] \\ 0 & \text{otherwise}\end{cases}$$
$$\text{with } q = |\boldsymbol{r}-\boldsymbol{r}'|/h \tag{2}$$

is a popular choice and also employed in the present work. The SPH discretization of (1) is then given by the so-called particle approximation

$$f(\boldsymbol{r}) \approx \sum_{|\boldsymbol{r}-\boldsymbol{r}_i|\leq 2h} f_i \frac{m_i}{\rho_i} W(|\boldsymbol{r}-\boldsymbol{r}_i|, h), \tag{3}$$

a sum over all particles which lie within the smoothing domain around $\boldsymbol{r}$, where f_i is the value of the field variable f associated with particle i, and m_i and ρ_i its mass and density, respectively. In 3D problems, the smoothing length h is typically chosen in the range of $[\Delta x, 1.5\Delta x]$, where Δx denotes the average particle spacing, resulting in approximately 40-100 particles within the smoothing domain.

Based on the unstructured interpolation (3), the governing equations of the considered problem are discretized, leading to a set of ordinary differential equations – the equations of motion – for the particles' positions and velocities $\boldsymbol{r}_i$ and $\boldsymbol{v}_i$, as well as equations for the regarding field variables with respect to time. The mass and relevant quantities move with the particles, in a way, material points, rendering SPH a meshless Lagrangian method.

The method originally evolved from the context of gas dynamics in astrophysical problems (see, e.g., Lucy (1977)) and later was applied to free surface flows by Monaghan (1994). Over the years, it has been successfully employed in various problems of solid and fluid mechanics, see, for instance, Monaghan (2005) or Liu and Liu (2010). Due to its meshfree Lagrangian character, SPH is well suited for complex flow problems involving free surfaces and time-dependent domains (such as fluid-structure interaction (Schörgenhumer et al. (2013)) or the flow and mixing in partially filled, complex geometries (Eitzlmayr and Khinast (2015)), since it neither requires to explicitly keep track of the free surface nor to employ mesh adaption or interpolation techniques to account for domains changing over time.

In order to study the sloshing problems in the present work, we apply the SPH discretization (3) to the Navier-Stokes equations for weakly-compressible isothermal Newtonian flows. The resulting equations of motion for each particle i read in their symmetrized form (for enhanced consistency)

$$\dot{\boldsymbol{r}}_i = \boldsymbol{v}_i$$
$$\dot{\boldsymbol{v}}_i = -\sum_{j,r_{ij}<2h} m_j \left(\frac{p_i}{\rho_i^2} + \frac{p_j}{\rho_j^2}\right) \nabla_i W(r_{ij}, h) + \frac{2\eta}{\rho_i} \sum_{j,r_{ij}<2h} \frac{m_j}{\rho_j} \boldsymbol{v}_{ij} \left(\frac{\boldsymbol{r}_{ij}}{|\boldsymbol{r}_{ij}|^2} \nabla_i W(r_{ij}, h)\right) + g \tag{4}$$

with $\boldsymbol{r}_i$, $\boldsymbol{v}_i$, p_i, ρ_i denoting the position, velocity, pressure, and density of particle i, respectively, η the dynamic viscosity, g the gravity, as well as $r_{ij} = |\boldsymbol{r}_i - \boldsymbol{r}_j|$ and $\boldsymbol{v}_{ij} = \boldsymbol{v}_i - \boldsymbol{v}_j$. The viscous terms are modelled according to Morris et al. (1997). The density is computed from the continuity equation

$$\dot{\rho}_i = \sum_{j,r_{ij}<2h} m_j \boldsymbol{v}_{ij} \nabla_i W(r_{ij}, h), \tag{5}$$

and the pressure is related to the density by the so-called Tait equation of state (cf. Monaghan (1994))

$$p_i(\rho_i) = \frac{c_0^2 \rho_0}{\gamma}\left(\left(\frac{\rho_i}{\rho_0}\right)^\gamma - 1\right), \tag{6}$$

where ρ_0 denotes the reference density, c_0 the speed of sound, and the constant γ typically chosen as 7. For further details on the derivation of (4)-(6), see, e.g., Monaghan (2005) or Liu and Liu (2010).

Two crucial aspects which complement above classical SPH formulation are explained in the following subsections and investigated in more detail in the present work – the modeling of wall boundary conditions, as well as smoothing and correction techniques for the density field in order to remove spurious noise and preserve stability and consistency.

2.2 Wall interaction models

If the fluid is in contact with a solid wall, two boundary conditions need to be fulfilled locally in each point on the interface, the so-called no-slip condition,

$$\boldsymbol{v}_{solid} = \boldsymbol{v}_{fluid} \tag{7}$$

and the equilibrium of forces,

$$\boldsymbol{\sigma}_{solid} = \boldsymbol{\sigma}_{fluid}, \tag{8}$$

with the local velocities $\boldsymbol{v}_{solid}$, $\boldsymbol{v}_{fluid}$ and stress tensors $\boldsymbol{\sigma}_{solid}$, $\boldsymbol{\sigma}_{fluid}$ of the solid and fluid domain, respectively. A range of different methods have been proposed to implement wall boundary conditions in SPH, for a detailed review see, e.g., Schörgenhumer (2016). In the present work, we employ and compare the following two approaches.

Firstly, hereinafter referred to as *(SPH) wall model A*, a force-field approach is considered where, in case an SPH

particle is sufficiently close (typically, within the range of Δx) to a boundary, repulsive and viscous penalty forces

$$\boldsymbol{f}_{rep} = \int_\Gamma \boldsymbol{\sigma}_r(\boldsymbol{r}_{rel})dS \quad \text{and} \quad \boldsymbol{f}_{visc} = \int_\Gamma \boldsymbol{\sigma}_v(\boldsymbol{r}_{rel}, \boldsymbol{v}_{rel})dS \quad (9)$$

are computed and applied as mutual interaction forces between the local wall elements and SPH particles, approximating the boundary conditions (7) and (8). In (9), $\boldsymbol{\sigma}_r$ and $\boldsymbol{\sigma}_v$ are short-ranged surface densities of repulsive and viscous forces, Γ is the fluid-solid interface, and $\boldsymbol{r}_{rel}$ and $\boldsymbol{v}_{rel}$, respectively, denote the relative position and velocity between the SPH particle and local integration points on Γ. The surface convolution integrals in (9) are computed numerically using Gauss-Legendre quadrature, based on discretized boundaries Γ by means of triangular STL meshes. For further details, cf. Schörgenhumer et al. (2013).

The second approach, in the following referred to as *(SPH) wall model B*, utilizes the idea of wall boundary particles, however, without actually including additional particles, but rather fitting their missing contributions by polynomials and adding them to the governing equations (4) and (5) for particles in the vicinity of walls (Eitzlmayr et al. (2014)). The terms added to the momentum equation (4) have the form

$$\dot{\boldsymbol{v}}_i^\Gamma = -\frac{m_i 2p_i}{\rho_i^2 h^4} F_{\nabla W} \boldsymbol{n}_i^\perp - \frac{m_i 2\eta \boldsymbol{v}_{i,rel}}{\rho_i^2 h^5}\left(1 + \frac{\Delta x}{2r_{i,rel}^\perp}\right) F_{\nabla W/r}\,, \quad (10)$$

and for the continuity equation, we have

$$\dot{\rho}_i^\Gamma = m_i v_i^\perp \frac{1}{h^4} F_{\nabla \mathrm{W}}\,, \quad (11)$$

where $\boldsymbol{n}_i^\perp$ denotes the wall normal direction, identified as the unit vector from SPH particle i to the closest point on the wall boundary Γ, $\boldsymbol{v}_{i,rel}$ denotes the velocity of particle i relative to the wall, $v_i^\perp$ the component of $\boldsymbol{v}_{i,rel}$ in direction $\boldsymbol{n}_i^\perp$, and $r_{i,rel}^\perp$ the shortest distance of particle i from the wall. The factors $F_{\nabla W}$ and $F_{\nabla W/r}$ contain 4-th order polynomial fits of the boundary particle contribution as a function of $r_{i,rel}^\perp$.

Equations (10) and (11) compensate for the fact that the kernel support domain of particles located within a distance of $2h$ from the wall is cut off, which leaves summation (3) incomplete and inconsistent due to the lack of neighbouring particles. In order to ensure that particles do not penetrate walls, an additional short-ranged repulsive force is implemented which acts along $\boldsymbol{n}_i^\perp$ between SPH particles and the nearest wall element. Complex boundary geometries again are represented by 3D triangular surface meshes.

Both wall models are tested and compared by the numerical examples described in Section 3.

2.3 Smoothing and corrections of the density field

An appropriate smoothing of the density field (typically, in intervals of 10-50 time steps) is essential in weakly-compressible SPH formulations in order to suppress spurious noise and retain numerical stability. In the present work, we utilize a first-order consistent moving least squares (MLS) filter where the smoothed density value ρ_i^* for particle i is computed from the linear system of equations

$$\boldsymbol{M} \cdot \left(\rho_i^*, \frac{\partial \rho_i^*}{\partial x}, \frac{\partial \rho_i^*}{\partial y}, \frac{\partial \rho_i^*}{\partial z}\right)^T = \boldsymbol{b} \quad \text{with}$$

$$\boldsymbol{b} = -\sum_{j, r_{ij}<2h} m_j W_{ij} \left(-1, x_{ij}, y_{ij}, z_{ij}\right)^T \quad \text{and}$$

$$\boldsymbol{M} = \sum_{j, r_{ij}<2h} \frac{m_j}{\rho_j} W_{ij} \begin{pmatrix} 1 & -x_{ij} & -y_{ij} & -z_{ij} \\ \vdots & x_{ij}^2 & x_{ij}y_{ij} & x_{ij}z_{ij} \\ \vdots & \ddots & y_{ij}^2 & y_{ij}z_{ij} \\ \text{sym.} & \dots & \dots & z_{ij}^2 \end{pmatrix}, \quad (12)$$

using $\left(x_{ij}, y_{ij}, z_{ij}\right)^T = \boldsymbol{r}_i - \boldsymbol{r}_j$ and $W_{ij} = W(r_{ij}, h)$. For a derivation of the MLS equations, see, e.g., Gomez-Gesteira (2010). In each smoothing step, the linear system (12) is solved and ρ_i replaced by ρ_i^*. Above MLS filter is first-order consistent, i.e., it reproduces and thus, also conserves linear density or pressure fields – or constant gradients – exactly, in contrast to the well-known Shepard filter (cf., e.g., Gomez-Gesteira (2010)) which is just zero-order consistent and gradually removes any kind of gradient. Only in case of an ill-conditioned system (12), which may occur if a particle is isolated or has only very few neighbors within its smoothing domain, ρ_i^* is replaced by the corresponding Shepard interpolant $(\boldsymbol{b})_1/(\boldsymbol{M})_{11}$ (with the subscript indices denoting the corresponding components of $\boldsymbol{b}$ and $\boldsymbol{M}$).

The second important extension of the SPH formulation employed in the present work is a correction of the density field to preserve the volume of the fluid, i.e., the domain occupied by the SPH particles. Note that neither the integration of the continuity equation (5) nor above density filters strictly establishes the consistent relation between the volume occupied by the SPH particles, the corresponding mass distribution, and the density field. This deficiency was also reported by Eitzlmayr et al. (2017), who proposed a density correction in order to preserve the complete filling of a closed compartment with constant volume, which was achieved by a periodical, uniform shift of the density field, i.e., without affecting the gradients. For free surface flows, however, an extension of that technique is required. The density summation, i.e., the computation of ρ_i by

$$\rho_i = \rho_i^{sum} = \sum_{j, r_{ij}<2h} m_j W(r_{ij}, h) \quad (13)$$

instead of (5) would establish a consistent relation between spatial mass distribution and the density field (see Schörgenhumer (2016)), however, is not feasible due to significant problems in case of uneven particle distributions and missing contributions in the vicinity of domain boundaries. Although we still use (5) to compute the density field in the present work, we utilize the properties of (13) and propose the following correction for volume conservation. After each application of the MLS density filter, the average summation density as well as the average actual density over all N particles are computed,

$$\rho_{avg}^{sum} = \frac{1}{N}\sum_{i=1}^N \rho_i^{sum} \quad \text{and} \quad \rho_{avg} = \frac{1}{N}\sum_{i=1}^N \rho_i\,, \quad (14)$$

and subsequently, the density field is shifted to corrected values, similar to Eitzlmayr et al. (2017)

$$\rho_i^{corr} = \rho_i + (\rho_{avg}^{sum} - \rho_{avg}). \quad (15)$$

Shifting the density field according to (15) enhances the conservation of volume significantly, while density and pressure gradients are preserved and errors due to inconsistencies in the vicinity of boundaries or free surfaces (as discussed above, owed to the density summation approach (13)) are small. The properties and importance of both appropriate density smoothing as well as the proposed extension for volume conservation are demonstrated by the test cases in the following section.

3. RESULTS AND DISCUSSION

The approach was applied to several examples from recent studies in literature in which both measurement data as well as results from analytical and numerical models are provided. The SPH formulation described in Section 2 is implemented within the particle simulation code LIGGGHTS (cf. CFDEM (2019)) which is coupled with the simulation tool HOTINT for mechatronic and multi-physics problems (see, e.g., Gerstmayr et al. (2013), HOTINT (2019)) to perform the coupled simulations and analysis of the sloshing problems.

3.1 Test Case 1 – Moriello et al. (2018)

In the first example, a liquid handling robotic system is considered. Goal in the original work by Moriello et al. (2018) is to suppress sloshing in point-to-point motions of liquid-filled vessels. To this end, a simplified analytical pendulum model was employed for the control strategy, and measurements regarding the frequencies and damping of the first sloshing mode (depending on the filling level of the container), as well as the sloshing dynamics for given trajectories were conducted. In the experiments, a cylindrical container with a radius of 97.5 mm was filled with 1, 2, and 3 liters of water (dynamic viscosity close to 1 mPa·s) and a trajectory along a straight line parallel to the ground was defined by the velocity profile shown in Fig.1.

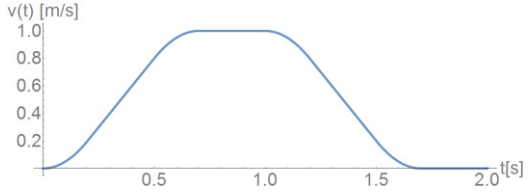

Fig. 1. Velocity profile of the test trajectory.

The presented numerical approach was applied to this use case – for illustration, see a snapshot of the simulation in Fig. 2 – and studied with respect to the influence of the wall model, density smoothing and corrections, spatial resolution and smoothing discretization (determined by the ratio $h/\Delta x$).

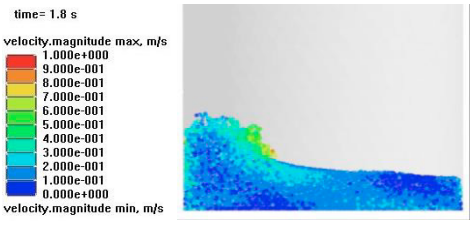

Fig. 2. Snapshot of a simulation with a filling quantity of 1 liter at $t = 1.8\ s$, using a discretization of ≈37000 particles and wall model B (cf. Subsection 2.2).

As default SPH setup, we used the Wendland kernel (2), a relatively coarse spatial resolution (amounting to ≈15000 particles for 1 liter of water) and $h/\Delta x = 1.25$ (resulting in ≈65 particles within the kernel support domain), combined with the MLS filter (12) and density correction (15) in intervals of 40 time steps. For the equation of state (6), the parameters were chosen as ρ_0=1000 kg/m³, $\gamma = 7$, and c_0 = 3 m/s, such that the density variations remained within a few percent (see also Monaghan (1994)).

First, a comparison of the resulting sloshing forces on the container was evaluated for the two SPH wall models and two different ratios of $h/\Delta x$ with constant Δx. All other settings were identical and chosen as described above. Note that reduced analytical models, such as the pendulum model in Moriello et al. (2018), often cannot provide forces without calibration against measurements or resolved numerical simulation models.

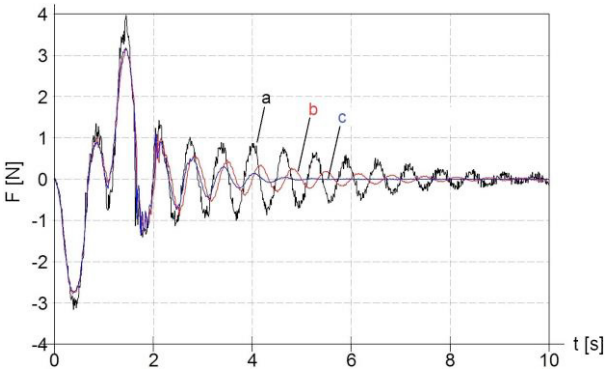

Fig. 3. Forces on the container due to the sloshing motion over time for three different model configurations. Black line (a): wall model B, $h/\Delta x = 1.25$. Red line (b): wall model A, $h/\Delta x = 1.25$. Blue line (c): wall model A, $h/\Delta x = 1.0$.

As shown in Fig. 3, whereas the frequency of the dominant sloshing mode as well as the forces during the initial motion phase of the container are predicted comparably well in all three cases, the numerical damping crucially depends on the model settings. We observed that wall model B (cf. line (a) in Fig. 3) generally introduces significantly less damping than wall model A (lines (b) and (c) in Fig. 3), however, with a larger amount of noise in the resulting forces. This can be explained by the inconsistencies introduced by wall model A in the vicinity of boundaries. Even though the penalty forces (9) approximate the conditions (7) and (8), the repulsive and viscous terms are not consistent with the SPH formulation and there is no contribution to the density (and pressure) field which also leads to artefacts such as overly dense layers of particles adjacent to the walls. If an SPH particle approaches a solid boundary, the repulsive force prevents penetration and establishes a balance of forces, however, the particle's density and pressure lack their contributions from the missing neighbour particles across the wall boundary, as opposed to the characteristics of wall model B. We assume that these inconsistencies, combined with the viscous penalty terms, lead to excessive dissipation. On the other hand, regarding the smoothness of the forces, wall model B directly couples not only particle positions, but also the pressure values with the wall interaction, which tends to produce more noise as

compared to wall model A's integral penalty terms. Furthermore, increasing the ratio $h/\Delta x$ by increasing h – which increases the smoothing error in (1), however, decreases the discretization error of (3) compared to (1) due to a higher number of particles within the kernel support domain – significantly reduces the damping effects (cf. line (b) vs. (c) in Fig. 3). That effect was mainly observed for wall model A, while the results for B were almost independent on $h/\Delta x$. The origin for this is yet unclear. Note that, in all cases, the same viscosity model and parameters were used for the fluid, and even the least dissipative case showed higher numerical damping than the experimental results. A more thorough analysis of the complex dissipation processes is subject to future work. Recent studies already deal with the issue of dissipation and long-duration stability, see, e.g., Green and Peiró (2018) in the context of tank sloshing.

Next, the resulting frequency of the dominant sloshing mode was investigated depending on the wall model, the spatial resolution (Δx), and the size of the smoothing domain ($h/\Delta x$). The results for a filling quantity of 1 liter are summarized in Table 1. Even with relatively coarse resolutions (small numbers of particles), satisfactory agreement with the measurements was obtained, particularly in case of wall model B which deviates only a few percent from the experimental reference $f_{exp} = 1.65$ Hz. Similar results were found also for higher filling quantities.

Table 1. Frequencies f_A and f_B of the first sloshing mode with a filling quantity of 1 liter for wall models A and B, in dependence of h and Δx. $f_{exp} = 1.65$ Hz is the reference value obtained from experiments in Moriello et al. (2018).

Δx [mm]	# particles	$h/\Delta x$	f_A/f_{exp}	f_B/f_{exp}
3	37037	1.25	0.934	0.981
4	15625	1.25	0.915	0.979
5	8000	1.25	0.908	0.966
4	15625	1.0	0.969	0.995
4	15625	1.5	0.888	0.973

Wall model A generally yields smaller frequencies, which is due to the significantly higher numerical damping as compared to wall model B, cf. again above discussion as well as Fig. 3. As expected, convergence towards the experimental results can be observed with higher spatial resolutions (i.e., smaller Δx). Conversely, increasing the ratio $h/\Delta x$ leads to (slightly) smaller frequencies, whereas the damping is reduced. That finding is subject to further investigation.

Finally, a study regarding the smoothing and consistency of the density field has been conducted for long-duration simulations, for illustration, see Fig. 4. The combination of the first-order consistent MLS filter (12) with the volume correction (15) produced the desired behavior, i.e., the both a consistent density and pressure field (cf. the linear hydrostatic profile in Fig. 4(a)) as well as the conservation of volume. The (zero-order consistent) Shepard filter, expectedly, gradually leads to inconsistent constant pressure fields and volumes (cf. Fig. 4(b), even if (15) is employed. Omitting the correction (15) for volume preservation, no long-term stable results could be achieved (Fig. 4(c)). In conclusion, consistent smoothing and correction techniques for the density field are essential to obtain satisfactory results, particularly in long-duration simulations. One alternative to the presented method would be the so-called δ-SPH schemes, see, e.g., Green and Peiró (2018) for further reading.

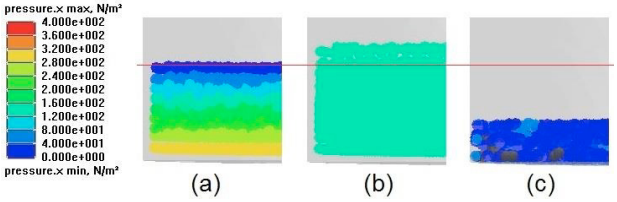

Fig. 4. Stationary solution for the container at rest after 60s simulated time using (a) the MLS filter (12) with correction (15), (b) the Shepard filter with correction, and (c) the MLS filter without correction. The red line indicates the target filling height. The hydrostatic target pressure at the bottom lies around 330 N/m².

3.2 Test Case 2 – Battaglia et al. (2018)

In the second example, the frequency response of the wave amplitude in steady-state sloshing in rectangular tanks with harmonic excitation was investigated. For details regarding the experimental setup, see Battaglia et al. (2018). Fig. 5 shows the results obtained with both SPH wall models compared to measurements. The findings are in agreement with those of the previous example – both wall models yield satisfactory results, model B is very close to the experimental reference, whereas model A leads to smaller wave heights and frequencies due to its higher numerical damping.

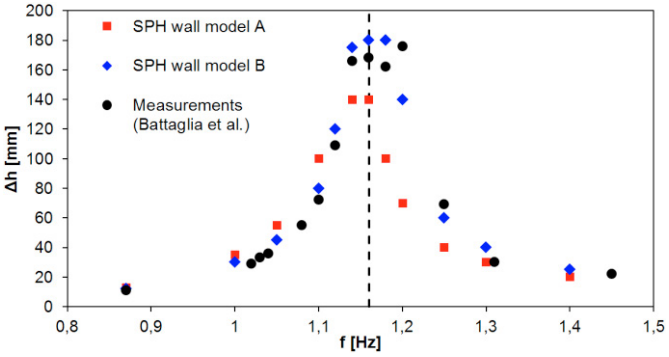

Fig. 5. Frequency response of the wave height Δh (difference maximum – minimum height) in steady-state tank sloshing with harmonic excitation of the first sloshing mode.

4. CONCLUSIONS

The proposed numerical approach for the model-based analysis of sloshing problems has shown promising results. Regarding the underlying SPH formulation, the modelling of solid wall boundary conditions as well as the consistent treatment of the density field have proven to be of crucial importance. Specific aspects, particularly regarding stability, smoothness, and consistency in vicinity of walls, as well as numerical dissipation are subject to further investigation.

Currently, an automated test bed including a camera as well as force sensors for the detailed experimental analysis of sloshing in liquid-filled vessels is under construction. The

measurements shall also serve for calibration and validation of the simulation models. The future goal of these research activities is to develop and calibrate reduced real-time-capable models based on both resolved numerical simulations as well as experimental data, and study their applicability and potential, with the overall motivation of implementing the reduced models within soft-and hardware frameworks in the field of automation, see also Zehetleitner et al. (2019).

ACKNOWLEDGEMENTS

This work has been supported by the LCM – K2 Center within the framework of the Austrian COMET-K2 program.

REFERENCES

Battaglia, L., Cruchaga, M., Storti, M., D'Elía, J., Aedo, J. N., and Reinoso, R. (2018). Numerical modelling of 3D sloshing experiments in rectangular tanks. *Applied Mathematical Modelling*, 59, 357-378.

CFDEM (2019) – *Open Source CFD, DEM, and CFD-DEM*. https://www.cfdem.com/liggghtsr-open-source-discrete-element-method-particle-simulation-code.

Chentanez, N., and Müller, M. (2011). Real-time Eulerian water simulation using a restricted tall cell grid. In *ACM Transactions on Graphics* (Vol. 30, No. 4, p. 82). ACM.

Eitzlmayr, A., Koscher, G., and Khinast, J. (2014). A novel method for modeling of complex wall geometries in smoothed particle hydrodynamics. *Computer Physics Communications*, 185(10), 2436-2448.

Eitzlmayr, A., and Khinast, J. (2015). Co-rotating twin-screw extruders: Detailed analysis of conveying elements based on smoothed particle hydrodynamics. Part 1: Hydrodynamics. *Chemical Engineering Science*, 134, 861-879.

Eitzlmayr, A., Matic, J., Khinast, J. (2017). Analysis of Flow and Mixing in Screw Elements of Corotating Twin-Screw Extruders via SPH. *AIChE Journal* 63(6), 2451-2463.

Fonfach, J. M., Manderbacka, T., and Neves, M. A. S. (2016). Numerical sloshing simulations: Comparison between lagrangian and lumped mass models applied to two compartments with mass transfer. *Ocean Engineering*, 114, 168-184.

Gao, H., Kwok, K. C. S., and Samali, B. (1997). Optimization of tuned liquid column dampers. *Engineering Structures*, 19(6), 476-486.

Gerstmayr, J., Dorninger, A., Eder, R., Gruber, P., Reischl, D., Saxinger, M., ... and Vetyukov, Y. (2013). Hotint: A script language based framework for the simulation of multibody dynamics systems. In *ASME 2013 IDETC CIE Conference* (pp. V07BT10A047-V07BT10A047). American Society of Mechanical Engineers.

Gomez-Gesteira, M., Rogers, B. D., Dalrymple, R. A., and Crespo, A. J. (2010). State-of-the-art of classical SPH for free-surface flows. *Journal of Hydraulic Research*, 48(S1), 6-27.

Green, M. D., and Peiró, J. (2018). Long duration SPH simulations of sloshing in tanks with a low fill ratio and high stretching. *Computers & Fluids*, 174, 179-199.

HOTINT (2019) – *A flexible multibody system dynamics freeware code in C++*. https://hotint.lcm.at/.

Ibrahim, R. A. (2005). *Liquid sloshing dynamics: theory and applications*. Cambridge University Press.

Ibrahim, R. A., Pilipchuk, V. N., and Ikeda, T. (2001). Recent advances in liquid sloshing dynamics. *Applied Mechanics Reviews*, 54(2), 133-199.

Konopka, M., De Rose, F., Strauch, H., Jetzschmann, C., Darkow, N., and Gerstmann, J. (2018). Active slosh control and damping-Simulation and experiment. *Acta Astronautica*.

Liu, M. B., and Liu, G. R. (2010). Smoothed particle hydrodynamics (SPH): an overview and recent developments. *Archives of Computational Methods in Engineering*, 17(1), 25-76.

Lucy, L. B. (1977). A numerical approach to the testing of the fission hypothesis. *The Astronomical Journal*, 82, 1013-1024.

Monaghan, J. J. (1994). Simulating free surface flows with SPH. *Journal of Computational Physics*, 110(2), 399-406.

Monaghan, J. J. (2005). Smoothed particle hydrodynamics. *Reports on Progress in Physics*, 68(8), 1703.

Moriello, L., Biagiotti, L., Melchiorri, C., and Paoli, A. (2018). Manipulating liquids with robots: A sloshing-free solution. *Control Engineering Practice*, 78, 129-141.

Morris, J. P., Fox, P. J., and Zhu, Y. (1997). Modeling low Reynolds number incompressible flows using SPH. *Journal of Computational Physics*, 136(1), 214-226.

Rebouillat, S., and Liksonov, D. (2010). Fluid–structure interaction in partially filled liquid containers: a comparative review of numerical approaches. *Computers & Fluids*, 39(5), 739-746.

Schörgenhumer, M. (2016). *Smoothed Particle Hydrodynamics with Consistent Boundaries for Fluid-Structure Interaction*, No. 33 in Schriftenreihe Advances in Mechatronics. Trauner Verlag, Linz, Austria.

Schörgenhumer, M., Gruber, P. G., and Gerstmayr, J. (2013). Interaction of flexible multibody systems with fluids analyzed by means of smoothed particle hydrodynamics. *Multibody System Dynamics*, 30(1), 53-76.

Schörgenhumer, M., and Humer, A. (2018). Smoothed particle hydrodynamics and modal reduction for efficient fluid–structure interaction. *Mathematical and Computer Modelling of Dynamical Systems*, 24(4), 401-425.

Shao, J. R., Li, H. Q., Liu, G. R., and Liu, M. B. (2012). An improved SPH method for modeling liquid sloshing dynamics. *Computers & Structures*, 100, 18-26.

Toumi, M., Bouazara, M., and Richard, M. J. (2009). Impact of liquid sloshing on the behaviour of vehicles carrying liquid cargo. *European Journal of Mechanics-A/Solids*, 28(5), 1026-1034.

Yano, K. I., and Terashima, K. (2001). Robust liquid container transfer control for complete sloshing suppression. *IEEE Transactions on Control Systems Technology*, 9(3), 483-493.

Zehetleitner, K. and Klopf, Ch. and Schröck, J. (2019) Model based development of fluid transport systems for industrial applications. Submitted to: *Proceedings of the IFAC MECHATRONICS 2019 and NOLCOS 2019 symposium.*